

Intense paramagnon excitations in a large family of high-temperature superconductors

M. Le Tacon,¹ G. Ghiringhelli,² J. Chaloupka,¹ M. Moretti Sala,² V. Hinkov,^{1,3} M. W. Haverkort,¹
M. Minola,² M. Bakr,¹ K. J. Zhou,⁴ S. Blanco-Canosa,¹ C. Monney,⁴ Y. T. Song,¹ G. L. Sun,¹ C. T.
Lin,¹ G. M. De Luca,⁵ M. Salluzzo,⁵ G. Khaliullin,¹ T. Schmitt,⁴ L. Braicovich,² and B. Keimer¹

¹*Max Planck Institute for Solid State Research, 70569 Stuttgart, Germany*

²*CNR-SPIN, Dipartimento di Fisica, Politecnico di Milano, I-20133 Milano, Italy*

³*Department of Physics and Astronomy, University of British Columbia, Vancouver, Canada V6T1Z1*

⁴*Swiss Light Source, Paul Scherrer Institut, CH-5232 Villigen PSI, Switzerland*

⁵*CNR-SPIN, Complesso Monte Santangelo via Cinthia, I-80126 Napoli, Italy*

In the search for the mechanism of high-temperature superconductivity, intense research has been focused on the evolution of the spin excitation spectrum upon doping from the antiferromagnetic insulating to the superconducting states of the cuprates.¹⁻³ Because of technical limitations, the experimental investigation of doped cuprates has been largely focused on low-energy excitations in a small range of momentum space.⁵⁻¹² Here we use resonant inelastic x-ray scattering¹³⁻¹⁶ to show that a large family of superconductors, encompassing underdoped $\text{YBa}_2\text{Cu}_4\text{O}_8$ and overdoped $\text{YBa}_2\text{Cu}_3\text{O}_7$, exhibits damped spin excitations (paramagnons) with dispersions and spectral weights closely similar to those of magnons in undoped cuprates. The comprehensive experimental description of this surprisingly simple spectrum permits quantitative tests of magnetic Cooper pairing models. A numerical solution of the Eliashberg equations for the magnetic spectrum of $\text{YBa}_2\text{Cu}_3\text{O}_7$ reproduces its superconducting transition temperature within a factor of two, a level of agreement comparable to Eliashberg theories of conventional superconductors.¹⁷

The twenty-fifth anniversary of the discovery of high-temperature superconductivity is approaching without a clear and compelling theory of the mechanism underlying this phenomenon. After the discovery of an unconventional (*d*-wave) symmetry of the Cooper pair wave function in the copper oxides, the thrust of research has been focused on the role of repulsive Coulomb interactions between conduction electrons, which naturally explain this pairing symmetry. However, since even simple models based on repulsive interactions have thus far defied a full solution, the question of whether such interactions alone can generate high-temperature superconductivity is still open. A complementary, more empirical approach has asked whether antiferromagnetic spin fluctuations, which are a generic consequence of Coulomb interactions, can mediate Cooper pairing in analogy to the phonon-mediated pairing mechanism in conventional superconductors.¹ This scenario requires the existence of well-defined antiferromagnetic spin fluctuations in the superconducting range of the cuprate phase diagram (for mobile hole concentrations $5\% \leq p \leq 25\%$ per copper atom), well outside the narrow stability range of antiferromagnetic long-range order ($0 \leq p \leq 2\%$).

An extensive series of experiments using inelastic spin-flip scattering of neutrons has indeed revealed low-energy spin fluctuations in doped cuprates.² Signatures of coupling between spin and charge excitations have also been identified,³ and evidence has been reported that this coupling is strong enough to mediate superconductivity in underdoped cuprates.⁴ However, for cuprate compounds hosting the most robust superconducting states, namely those that are optimally doped to exhibit $T_c \geq 90$ K, inelastic neutron scattering (INS) experiments have thus far mostly revealed spin excitations over a narrow range of excitation energies $E \sim 30 - 70$ meV, wave vectors \mathbf{Q} covering only $\sim 10\%$ of the Brillouin zone area around the antiferromagnetic ordering wave vector \mathbf{Q}_{AF} , and temperatures $T < T_c$.⁵⁻¹² The energy- and momentum-integrated intensity of these excitations constitutes only a few percent of the spectral weight of spin waves in antiferromagnetically ordered cuprates,^{3,18} and is thus clearly insufficient to support high- T_c superconductivity. Although the recent discovery of a weakly dispersive magnetic excitation in the model system $\text{HgBa}_2\text{CuO}_{4+\delta}$ with $E \sim 50$ meV may account for some of the missing spectral weight,¹⁹ the apparent weakness of antiferromagnetic fluctuations in optimally doped compounds has been used as a central argument against magnetically mediated pairing scenarios for the cuprates.²⁰

This picture is, however, strongly influenced by technical limitations of the INS method that arise from the small cross section of magnetic neutron scattering in combination with the weak

primary flux of currently available high-energy neutron beams. Because of intensity constraints, even the detection of undamped spin waves in antiferromagnetically ordered cuprates over their full band width of ~ 300 meV has required single-crystal samples with volumes of order 10 cm^3 , which are very difficult to obtain.^{21–24} Doping further reduces the intensity of the INS profiles and exacerbates these difficulties.

Here we take advantage of recent progress in the development of high-resolution resonant inelastic x-ray scattering (RIXS) in order to explore magnetic excitations in a wide energy-momentum window that has been largely hidden from view by INS. Experiments on undoped cuprates have shown that RIXS with photon energies at the Cu L_3 absorption edge is sensitive to single-magnon excitations^{13–16} by virtue of the strong spin-orbit coupling of the $2p_{3/2}$ core-hole intermediate state,^{25,26} in excellent agreement with INS measurements.^{24,27} Initial RIXS experiments on doped $\text{La}_{2-x}\text{Sr}_x\text{CuO}_4$ have revealed a complex two-component lineshape with excitations extending up to about 350 meV; the presence of two branches was attributed to phase separation between the superconducting state and a competing state with incommensurate spin and charge order.²⁷ We have applied the same method to $\text{YBa}_2\text{Cu}_3\text{O}_{6+x}$ (YBCO_{6+x}), $\text{Nd}_{1.2}\text{Ba}_{1.8}\text{Cu}_3\text{O}_{6+x}$ (NdBCO_{6+x}), and $\text{YBa}_2\text{Cu}_4\text{O}_8$, which are much less affected by doping-induced disorder and do not show phase separation.²⁸

Although one cannot reach Q_{AF} with RIXS, one of its great advantages over INS is that it allows measurements of magnetic excitations with sizable intensity over much of the accessible reciprocal space, even on very small sample volumes. The results presented here have been obtained on thin films and on millimeter-sized single crystals far below the volume requirements of INS (see Supplementary Information). Figure 1 shows a sketch of the scattering geometry of our experiment, as well as RIXS spectra obtained on undoped antiferromagnetic NdBCO_6 (Fig. 1 c,d) and underdoped superconducting NdBCO_7 (Fig. 1 f,g), for incident photon polarizations in and out of the scattering plane (π and σ geometries) and a momentum transfer $q_{//}$ along the reciprocal-space a^* direction corresponding to 0.37 reciprocal lattice units (r.l.u.). For both scattering geometries, the spectra exhibit an intense peak located around 1.7 eV energy loss that arises from optically forbidden \underline{dd} excitations (that is, transitions of the unpaired hole of Cu^{2+} from the $d_{x^2-y^2}$ to other d orbitals)²⁹ on top of a continuum of charge-transfer excitations. At lower energies, we can see in both compounds an inelastic feature centered around 250 meV and a resolution-limited elastic peak.

For undoped antiferromagnetic NdBCO_6 , we can decompose the response in the mid-

infrared (MIR) region of the spectra (Fig. 1e) for energy losses below ~ 500 meV following the method employed in Ref. 27. In the π scattering geometry, this leads to (i) an intense resolution-limited peak around 250 meV, (ii) a high-energy tail of this peak centered around 400 meV, and (iii) a weak low-energy contribution around 100 meV. In the σ scattering geometry, feature (i) is strongly suppressed. This polarization dependence allows us to assign this feature to a single-magnon excitation, in agreement with theoretical considerations^{16,25} and previous investigations on other cuprates.^{14–16,27} This assignment is further confirmed by the disappearance of the MIR inelastic response as the incident photon energy is moved away from the Cu- L_3 absorption edge (not shown). The weak features (ii) and (iii) are associated with higher-order spin excitations and lattice vibrations (single and multiple phonon excitations that are not individually resolved), respectively.

The energy of the single-magnon feature in NdBCO₆ depends strongly on $q_{//}$ (left panel of Fig. 2). Since the lineshape of the MIR spectrum is $q_{//}$ -independent, the fitting procedure described above can be used to obtain the magnon dispersion relation. The result displayed in Fig. 3a is clearly different from the sinusoidal magnon dispersion observed in La₂CuO₄.^{24,27} Indeed, due to the presence of two antiferromagnetically coupled CuO₂ layers per unit cell, two magnon branches with different spin precession patterns are expected^{21–23} for NdBCO₆: an acoustic branch with intensity $\propto \sin^2(\frac{dq_{\perp}}{2})$, where q_{\perp} is the momentum transfer perpendicular to the CuO₂ layers and d is the spacing between the two CuO₂ layers, and an optical branch with intensity $\propto \cos^2(\frac{dq_{\perp}}{2})$. The result of the calculation of the relative intensities of these two branches for our scattering geometry is displayed in the inset of Fig. 3a. It shows that close to the Brillouin zone center the gapped optical branch dominates. Fitting our data using the spin-wave dispersion calculated for a bilayer in the framework of a simple Heisenberg model,^{21–23} we obtain $J_{//}=133 \pm 2$ meV and $J_{\perp}=12 \pm 3$ meV for the intra- and inter-layer exchange constants, respectively, in excellent agreement with the values obtained in antiferromagnetic YBCO_{6+x}.^{22,23}

We now turn to the doped systems. Figure 2 provides a synopsis of the experimental spectra for all systems investigated here, which span a wide range of doping levels: undoped NdBCO₆, strongly underdoped NdBCO₇ and YBCO_{6.6} ($T_c = 65$ K and 61 K, respectively), weakly underdoped YBa₂Cu₄O₈ ($T_c = 80$ K), and weakly overdoped YBCO₇ ($T_c = 90$ K). Because of their stoichiometric composition and electronic homogeneity, the latter two compounds have served as model compounds in the experimental literature on high- T_c superconductivity, but

apart from the “resonant mode” that appears in YBCO₇ below T_c ⁵ no information has been available on their magnetic excitation spectra. Fig. 2 shows that broad MIR features are present at all doping levels in the same energy range as the single-magnon peak in undoped NdBCO₆. Since these features obey the same polarization dependence as the magnon mode (Figs. 1 f,h), they can be assigned to magnetic excitations.

Based on the metallic nature of the doped cuprates, one expects strong damping of magnetic excitations in the Stoner continuum of incoherent electron-hole excitations. We have therefore fitted these spectra to Voigt profiles that are the result of the convolution of the Lorentzian lineshape of excitations with finite lifetime with the Gaussian resolution function. Since the fits yield excellent agreement with this simple profile (solid lines in Figs. 1 and 2), we can accurately extract the energies and half-widths-at-half-maximum (HWHM) of the magnetic excitation as a function of the transferred momentum (Fig. 3b,c). Before discussing these results, it is interesting to compare them to those previously reported on underdoped La_{2-x}Sr_xCuO₄.²⁷ As no double-peak structure is observed here, our data confirm the absence of phase separation in the YBCO and NdBCO families of compounds.²⁸

The magnetic excitation energies of NdBCO₇, YBCO_{6.6}, and YBCO₇ at the Brillouin zone boundary are nearly identical to the ones found in NdBCO₆. This implies that the in-plane exchange constant $J_{//}$ is not as strongly renormalized with doping as previously suggested based on extrapolation of lower-energy INS data,³⁰⁻³² in agreement with the most recent INS findings on YBCO_{6.5} using high energy neutrons.³³ Upon approaching the Γ point ($q_{//} = 0$), we observe that the dispersion in the doped compounds is steeper than in NdBCO₆. Despite the fact that Γ and \mathbf{Q}_{AF} are no longer equivalent in the absence of magnetic long-range order, the RIXS data obtained on YBCO_{6.6} nicely extrapolate to the low-energy “hour glass” dispersion around \mathbf{Q}_{AF} previously extracted from INS data on samples prepared in an identical manner.³⁴ Since the slope of the upward-dispersing branch close to the magnetic zone center is flatter than the one of the antiferromagnetic spin-wave dispersion,^{30,34} this indicates the presence of an inflexion point in the dispersion of magnetic excitations in the doped compounds. We note that the situation seems somewhat different for YBa₂Cu₄O₈, where the energy of the magnetic excitations close to the zone boundary is significantly reduced compared to the other systems (~ 210 meV instead of ~ 300 meV), and the dispersion is flatter than in NdBCO₆. This may reflect different values of $J_{//}$ and J_{\perp} in this system, and deserves further investigation. The intrinsic HWHM of ~ 200 meV of the inelastic signal extracted from our data (Fig. 3c) is much

larger than the instrumental resolution and comparable to the magnon energies, indicating strong damping by Stoner excitations. The damping rate does not change substantially with $q_{//}$ and with doping. Finally, while it is not possible yet to obtain absolute magnetic intensities from RIXS data, we can extract the relative intensity of the RIXS profiles by integrating the inelastic signal in the MIR region (see Supplementary Information). Remarkably, the integrated intensity obtained in this way is conserved upon doping from the antiferromagnetic insulator to the slightly overdoped superconductor.

We have thus demonstrated the existence of paramagnons, *i.e.* damped but well-defined, dispersive magnetic excitations, deep in the Stoner continuum of cuprates with doping levels beyond optimal doping. Their spectral weights are similar to those of spin waves in the undoped, antiferromagnetically ordered parent material.

In order to obtain insight into the origin of this surprising observation, we have performed exact-diagonalization calculations of the $t - J$ Hamiltonian with $J/t = 0.3$ on finite-sized clusters, following the method proposed in Refs. 35–37. We used clusters with 18 and 20 spins arranged in various shapes to map the (H,K,0) reciprocal plane with sufficient momentum resolution (see Supplementary Information). The resulting spectra were convoluted by a Gaussian function with HWHM $0.1t$ in order to simulate the experimental resolution function. The calculated imaginary part of the spin susceptibility is shown in Fig. 4a for different hole concentrations. In the undoped case, one can observe two peaks in the imaginary part of the spin susceptibility: an intense peak corresponding to the single-magnon excitation, and a weaker feature at higher energy corresponding to higher-order processes. The single-magnon peak clearly disperses, although its energy is slightly above the value expected from linear spin-wave theory (dotted lines), due to the finite size of the cluster. In the inset of Fig. 4a, we present the energy-integrated magnetic intensity in the (H,K,0) reciprocal plane. As expected, the intensity for in the undoped situation is strongly peaked at \mathbf{Q}_{AF} , and rather uniformly distributed in the rest of the plane. As holes are added to the clusters, the magnetic spectral weight strongly decreases only around \mathbf{Q}_{AF} , but remains essentially constant everywhere else. This can also be seen in Fig. 4b, where the imaginary part of the energy-integrated spin susceptibility is plotted as a function of doping. The experimental and numerical data are thus in excellent agreement.

Armed with essentially complete knowledge of the spin fluctuation spectrum, and motivated by the agreement with the numerical data for the $t - J$ model, we now estimate the super-

conducting transition temperature T_c generated by a Cooper pairing mechanism in which the experimentally detected spin fluctuations play the role of bosonic glue. To this end, we have self-consistently solved the Eliashberg equations using the vertex function of the $t - J$ model³⁸ and the experimental spin fluctuation spectrum of YBCO₇ (inset in Fig. 4c), without adjustable parameters. Details are given in the Supplementary Information. Figure 4c shows the outcome of the calculation. The resulting T_c of 170 K is similar to the maximum T_c observed in the cuprates and to another recent estimate based on the comparison of INS and photoemission data on underdoped YBCO_{6+x}.⁴ The agreement with the experimentally observed T_c of YBCO₇ is satisfactory in view of the neglect of vertex corrections beyond Eliashberg theory and other simplifying assumptions in the calculation, and in view of a similar level of quantitative agreement reported for Eliashberg calculations of conventional low- T_c superconductors.¹⁷ In order to resolve the relative contribution of the strongly doping dependent region around \mathbf{Q}_{AF} and the high-energy part of the spin susceptibility revealed by RIXS to the pairing strength, we have introduced momentum cutoffs around \mathbf{Q}_{AF} in the calculation (Fig. 4c). Clearly, both low- and high-energy spin fluctuations contribute substantially to the pairing. In underdoped cuprates with lower gaps and stronger antiferromagnetic correlations, vertex corrections are expected to become essential,³⁹ reducing the T_c values calculated here. These corrections suppress coupling to magnons in the vicinity of \mathbf{Q}_{AF} , leaving the contribution of the higher-energy excitations as a vital source of pairing.

-
1. For a review, see Abanov, A., Chubukov, A. V. & Schmalian, J. Quantum-critical theory of the spin fermion model and its application to cuprates: normal state analysis. *Adv. Phys.* **52**, 119-218 (2003).
 2. For a review, see Birgeneau, R. J., Stock, C., Tranquada, J. M. & Yamada, K. Magnetic neutron scattering in hole-doped cuprate superconductors. *J. Phys. Soc. Jpn.* **75**, 111003 (2006).
 3. For a review, see Eschrig, M. The effect of collective spin-1 excitations on electronic spectra in high-T_c superconductors. *Adv. Phys.* **55**, 47-183 (2006).
 4. Dahm, T. *et al.* Strength of the spin-fluctuation-mediated pairing interaction in a high-temperature superconductor. *Nature Phys.* **5**, 217-221 (2009).
 5. Fong, H. F. *et al.* Polarized and unpolarized neutron-scattering study of the dynamical spin susceptibility of YBa₂Cu₃O₇. *Phys. Rev. B* **54**, 6708-6720 (1996).
 6. Hayden, S. M. *et al.* The structure of the high-energy spin excitations in a high-transition-temperature superconductor. *Nature* **429**, 531-534 (2004).
 7. Hinkov, V. *et al.* Two-dimensional geometry of spin excitations in the high-transition-temperature superconductor YBa₂Cu₃O_{6+x}. *Nature* **430**, 650-653 (2004).
 8. He, H. *et al.* Magnetic Resonant Mode in the Single-Layer High-Temperature Superconductor Tl₂Ba₂CuO_{6+δ}. *Science* **295**, 1045-1047 (2002).
 9. Fauqué, B. *et al.* Magnetic Order in the Pseudogap Phase of High-T_C Superconductors. *Phys. Rev. Lett.* **96**, 197001 (2006).
 10. Reznik, D. *et al.* Local-moment fluctuations in the optimally doped high- T_c superconductor YBa₂Cu₃O_{6.95}. *Phys. Rev. B* **78**, 132503 (2008).
 11. Xu, G. *et al.* Testing the itinerancy of spin dynamics in superconducting Bi₂Sr₂CaCu₂O_{8+δ}. *Nature Phys.* **5**, 642-646 (2009).
 12. Yu, G. *et al.* Magnetic resonance in the model high-temperature superconductor HgBa₂CuO_{4+δ}. *Phys. Rev. B* **81**, 064518 (2010).
 13. Braicovich, L. *et al.* Dispersion of Magnetic Excitations in the Cuprate La₂CuO₄ and CaCuO₂ Compounds Measured Using Resonant x-Ray Scattering. *Phys. Rev. Lett.* **102**, 167401 (2009).
 14. Schlappa, J. *et al.* Collective Magnetic Excitations in the Spin Ladder Sr₁₄Cu₂₄O₄₁ Measured Using High-Resolution Resonant Inelastic x-Ray Scattering. *Phys. Rev. Lett.* **103**, 047401 (2009).
 15. Guarise, M. *et al.* Measurement of Magnetic Excitations in the Two-Dimensional Antiferromagnetic

- $\text{Sr}_2\text{CuO}_2\text{Cl}_2$ Insulator Using Resonant x-Ray Scattering: Evidence for Extended Interactions. *Phys. Rev. Lett.* **105**, 157006 (2010).
16. Braicovich, L. *et al.* Momentum and polarization dependence of single-magnon spectral weight for Cu L_3 -edge resonant inelastic x-ray scattering from layered cuprates. *Phys. Rev. B* **81**, 174533 (2010).
 17. Carbotte, J.P. Properties of boson-exchange superconductors. *Rev. Mod. Phys.* **62**, 1027-1157 (1990).
 18. Kee, H.-Y., Kivelson, S. A. & Aeppli, G. Spin-1 Neutron Resonance Peak Cannot Account for Electronic Anomalies in the Cuprate Superconductors. *Phys. Rev. Lett.* **88**, 257002 (2002).
 19. Li, Y. *et al.* Hidden magnetic excitation in the pseudogap phase of a high- T_c superconductor. *Nature* **468**, 283-285 (2010).
 20. Maksimov, E. G., Kulić, M. L. & Dolgov, O. V. Bosonic Spectral Function and the Electron-Phonon Interaction in HTSC Cuprates. *Adv. Cond. Mat. Phys.* **2010**, 423725 (2010).
 21. Tranquada, J. M. *et al.* Neutron scattering study of magnetic excitations in $\text{YBa}_2\text{Cu}_3\text{O}_{6+x}$. *Phys. Rev. B* **40**, 4503-4516 (1989).
 22. Reznik, D. *et al.* Direct observation of optical magnons in $\text{YBa}_2\text{Cu}_3\text{O}_{6.2}$. *Phys. Rev. B* **53**, R14741-R14744 (1996).
 23. Hayden, S. M. *et al.* High-frequency spin waves in $\text{YBa}_2\text{Cu}_3\text{O}_{6.15}$. *Phys. Rev. B* **54**, R6905-R6908 (1996).
 24. Coldea, R. *et al.* Spin Waves and Electronic Interactions in La_2CuO_4 . *Phys. Rev. Lett.* **86**, 5377-5380 (2001).
 25. Ament, L. J. P. *et al.* Theoretical Demonstration of How the Dispersion of Magnetic Excitations in Cuprate Compounds can be Determined Using Resonant Inelastic x-Ray Scattering. *Phys. Rev. Lett.* **103**, 117003 (2009).
 26. Haverkort, M. W. Theory of Resonant Inelastic X-Ray Scattering by Collective Magnetic Excitations. *Phys. Rev. Lett.* **105**, 167404 (2010).
 27. Braicovich, L. *et al.* Magnetic Excitations and Phase Separation in the Underdoped $\text{La}_{2-x}\text{Sr}_x\text{CuO}_4$ Superconductor Measured by Resonant Inelastic X-Ray Scattering. *Phys. Rev. Lett.* **104**, 077002 (2010).
 28. Bobroff, J. *et al.* Absence of Static Phase Separation in the High T_c Cuprate $\text{YBa}_2\text{Cu}_3\text{O}_{6+y}$. *Phys. Rev. Lett.* **89**, 157002 (2002).
 29. Ghiringhelli, G. *et al.* Low Energy Electronic Excitations in the Layered Cuprates Studied by Copper

- L_3 Resonant Inelastic X-Ray Scattering. *Phys. Rev. Lett.* **92**, 117406 (2004).
30. Stock, C. *et al.* From incommensurate to dispersive spin-fluctuations: The high-energy inelastic spectrum in superconducting $\text{YBa}_2\text{Cu}_3\text{O}_{6.5}$. *Phys. Rev. B* **71**, 024522 (2005).
 31. Vignolle, B. *et al.* Two energy scales in the spin excitations of the high-temperature superconductor $\text{La}_{2-x}\text{Sr}_x\text{CuO}_4$. *Nature Phys.* **3**, 163-167 (2007).
 32. Lipscombe, O. J. *et al.* Emergence of Coherent Magnetic Excitations in the High Temperature Underdoped $\text{La}_{2-x}\text{Sr}_x\text{CuO}_4$ Superconductor at Low Temperatures. *Phys. Rev. Lett.* **102**, 167002 (2009).
 33. Stock, C. *et al.* Effect of the pseudogap on suppressing high energy inelastic neutron scattering in superconducting $\text{YBa}_2\text{Cu}_3\text{O}_{6.5}$. *Phys. Rev. B* **82**, 174505 (2010).
 34. Hinkov, V. *et al.* Spin dynamics in the pseudogap state of a high-temperature superconductor. *Nature Phys.* **3**, 780-785 (2007).
 35. Tohyama, T., Horsch, P. & Maekawa, S. Spin and Charge Dynamics of the t-J Model. *Phys. Rev. Lett.* **74**, 980-983 (1995).
 36. Eder, R., Ohta, Y. & Maekawa, S. Anomalous Spin and Charge Dynamics of the t-J Model at Low Doping. *Phys. Rev. Lett.* **74**, 5124-5127 (1995).
 37. Dagotto, E. Correlated electrons in high-temperature superconductors. *Rev. Mod. Phys.* **66**, 763-840 (1994).
 38. Prelovšek P. and Ramšak, A. Spectral functions and the pseudogap in the t-J model *Phys. Rev. B* **63**, 180506(R) (2001).
 39. Schrieffer, J. R. Ward's identity and the suppression of spin fluctuation superconductivity. *J. Low Temp. Phys.* **99**, 397-402 (1995).

Supplementary Information accompanies this paper on www.nature.com/nphys

Acknowledgements This work was performed at the ADDRESS beamline using the SAXES instrument jointly built by Paul Scherrer Institut (Villigen, Switzerland), Politecnico di Milano (Italy) and École polytechnique fédérale de Lausanne (Switzerland). Part of this research project has been supported by the European Commission under the 7th Framework Programme: Research Infrastructures (Grant Agreement Number 226716), and the European project SOPRANO under Marie Curie actions (Grant No. PITNGA-2008-214040).

Author Information Correspondence and requests for materials should be addressed to M. L. T.

(m.letacon@fkf.mpg.de) or B. K. (b.keimer@fkf.mpg.de).

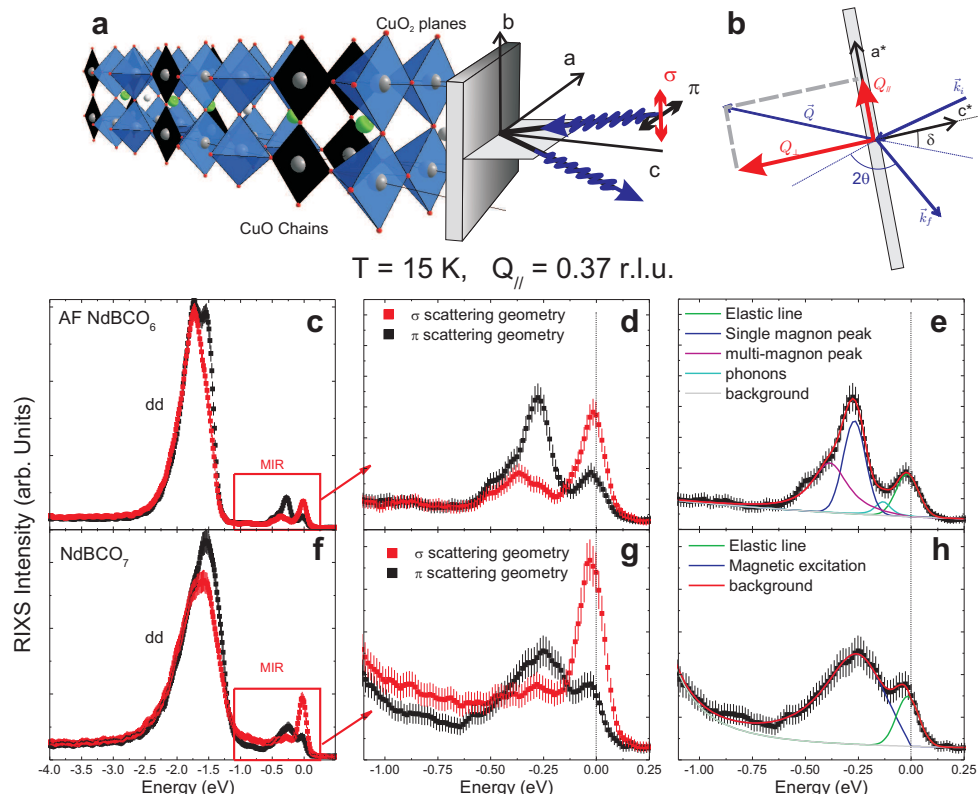


Fig. 1: a and b) Schematics of the scattering geometry. Typical RIXS spectra of undoped antiferromagnetic $\text{Nd}_{1.2}\text{Ba}_{1.8}\text{Cu}_3\text{O}_6$ (c, d, e) and superconducting underdoped $\text{Nd}_{1.2}\text{Ba}_{1.8}\text{Cu}_3\text{O}_7$ (f, g, h), obtained at $T = 15 \text{ K}$ for $q_{\parallel} = 0.37 \text{ r.l.u.}$, in both π (black squares) and σ (red squares) scattering geometries.

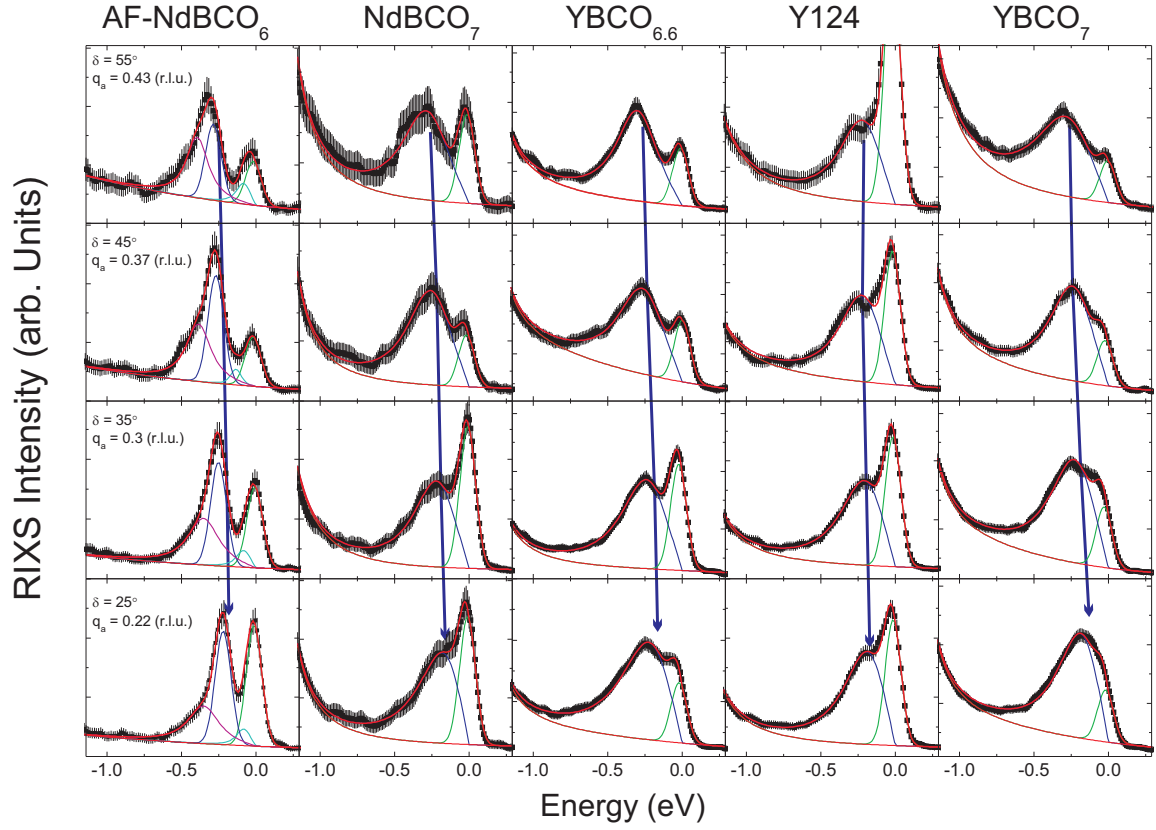


Fig. 2: RIXS response of undoped $\text{Nd}_{1.2}\text{Ba}_{1.8}\text{Cu}_3\text{O}_6$ (NdBCO_6), underdoped $\text{Nd}_{1.2}\text{Ba}_{1.8}\text{Cu}_3\text{O}_7$ (NdBCO_7), $\text{YBa}_2\text{Cu}_3\text{O}_{6.6}$ ($\text{YBCO}_{6.6}$), $\text{YBa}_2\text{Cu}_4\text{O}_8$, and slightly overdoped $\text{YBa}_2\text{Cu}_3\text{O}_7$ (YBCO_7) for various momentum transfers (see Fig. 1), at $T = 15$ K. Note that the spectra for NdBCO_7 were recorded for $\delta=20^\circ$, corresponding to $q_{//} = 0.18$ r.l.u.

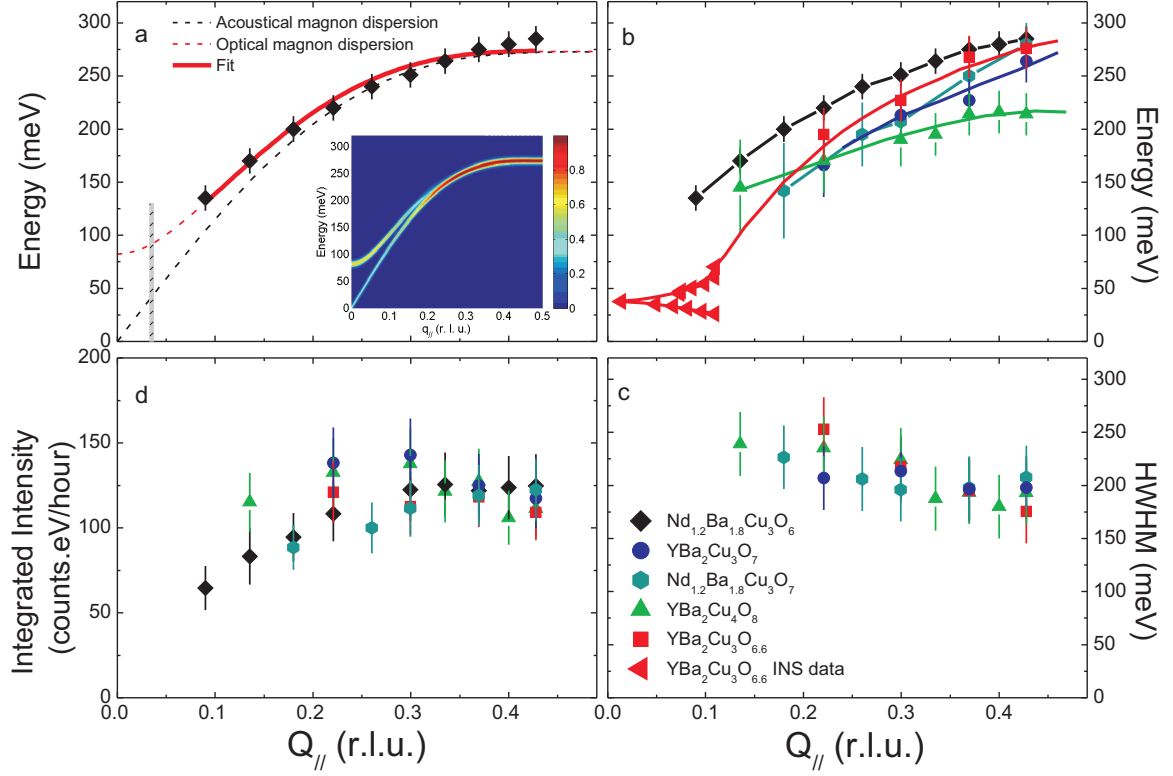


Fig. 3: a) Experimental magnon dispersion along 100 direction in AF $\text{Nd}_{1.2}\text{Ba}_{1.8}\text{Cu}_3\text{O}_6$ at $T = 15$ K, fitted using the spin-wave dispersion of a bilayer from Ref. 21 (thick red line). The dashed lines are the acoustical (black) and optical (red) spin wave dispersions calculated using the fitting parameters. The grey area represents our energy/momentum resolution. Inset: relative intensity of the acoustical and optical magnon for our scattering geometry. b) Experimental magnon dispersion along 100 direction in antiferromagnetic $\text{Nd}_{1.2}\text{Ba}_{1.8}\text{Cu}_3\text{O}_6$, underdoped $\text{Nd}_{1.2}\text{Ba}_{1.8}\text{Cu}_3\text{O}_7$, $\text{YBa}_2\text{Cu}_3\text{O}_{6.6}$, $\text{YBa}_2\text{Cu}_4\text{O}_8$ and $\text{YBa}_2\text{Cu}_3\text{O}_7$ at $T = 15$ K. Low-frequency INS data recorded along the 100 direction from (π, π) for $\text{YBa}_2\text{Cu}_3\text{O}_{6.6}$ have been added.³⁴ Lines are guides to the eye. c) HWHM of magnetic excitations in $\text{Nd}_{1.2}\text{Ba}_{1.8}\text{Cu}_3\text{O}_7$, $\text{YBa}_2\text{Cu}_3\text{O}_{6.6}$, $\text{YBa}_2\text{Cu}_4\text{O}_8$ and $\text{YBa}_2\text{Cu}_3\text{O}_7$. d) Integrated inelastic intensities (see also Supplementary Information).

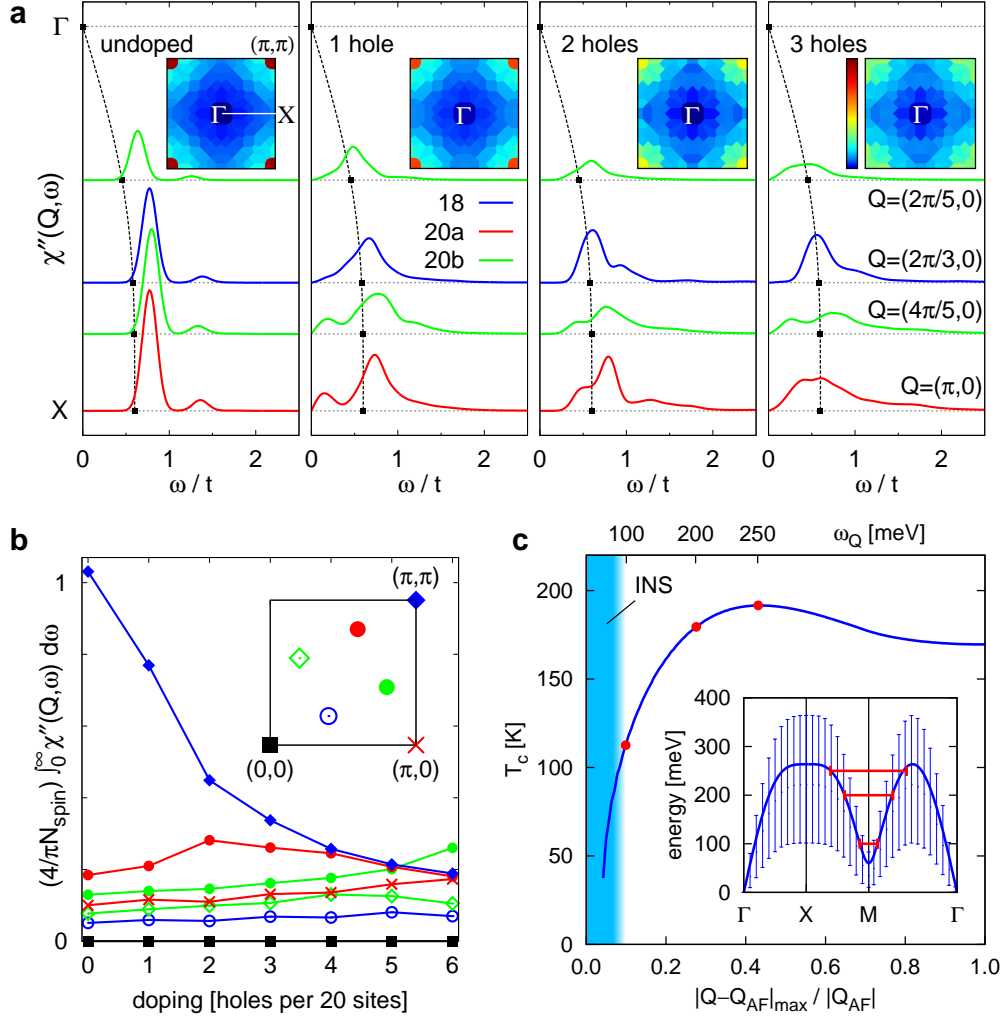


Fig. 4: a) Imaginary part of the spin susceptibility resulting from exact diagonalization of the $t - J$ model with $J/t = 0.3$ on small clusters. Results from 18-site and two 20-site clusters are combined to cover the $\Gamma - X$ line (see Supplementary Information). The spectra are broadened using a Gaussian with HWHM = $0.1t$. Dashed lines correspond to the linear spin wave dispersion with the same J as used in numerics. Insets: Brillouin-zone-maps of energy-integrated χ'' with a common color scale. b) Energy-integrated χ'' of the 20-site cluster, normalized to the number of electrons on the cluster, as a function of doping. The seven accessible non-equivalent \mathbf{q} -vectors for this cluster are shown in the inset. c) Superconducting transition temperature resulting from the Eliashberg calculation for the experimentally determined spin excitation spectrum of YBCO₇ displayed in the inset. The red marks indicate the influence of successive momentum-space cutoffs limiting the maximum distance from \mathbf{Q}_{AF} of the \mathbf{q} -vectors for which $\chi_{\mathbf{q}}(\omega)$ is included in the calculation.

Supplementary Information for
“Intense paramagnon excitations
in a large family of high-temperature superconductors”

Sample Preparation and Characterization

We used untwinned $\text{YBa}_2\text{Cu}_3\text{O}_{6.6}$ and $\text{YBa}_2\text{Cu}_3\text{O}_7$ single crystals of volume about $3 \times 3 \times 0.5 \text{ mm}^3$, with superconducting transition temperatures T_c of 61 K and 90 K ($\Delta T_c = 2 \text{ K}$), respectively, determined for each crystal by SQUID magnetometry (see details in Methods section of Ref. 1). The $\text{YBa}_2\text{Cu}_4\text{O}_8$ single crystals were obtained using KOH flux under ambient pressure in a box furnace. The source material was conventionally prepared polycrystalline $\text{YBa}_2\text{Cu}_3\text{O}_7$ mixed with CuO in a molar ratio of 1:1. The details are described in Refs. 2,3. The crystal size was $0.8 \times 0.8 \times 0.2 \text{ mm}^3$, and $T_c = 80 \text{ K}$. $\text{Nd}_{1.2}\text{Ba}_{1.8}\text{CuO}_{6+x}$ films of thickness 100 nm were deposited on SrTiO_3 (100) single crystals by diode high-pressure oxygen sputtering. The undoped $\text{Nd}_{1.2}\text{Ba}_{1.8}\text{CuO}_6$ film was obtained by annealing as-grown $\text{Nd}_{1.2}\text{Ba}_{1.8}\text{CuO}_7$ samples in Argon atmosphere (10 mbar) for 24 hours. Details of the film growth and characterization can be found in Ref. 4.

Table I lists the lattice parameters and transition temperatures of all samples.

Measurements

The RIXS measurements were performed at the ADRESS beam line⁵ of the Swiss Light Source (Paul Scherrer Institute, Switzerland) using the high-resolution SAXES spectrometer.⁶ The resonant conditions were achieved by tuning the energy of the incident x-ray to the maximum of the Cu L_3 absorption peak, around 931 eV. The total momentum transfer is 0.855 \AA^{-1} , which allows one to cover about 85% of the first Brillouin zone along the [100] direction (see Supplementary Figure 2). Momentum transfers are given in units of the reciprocal lattice vectors a^* , b^* and c^* where $a^* = 2\pi/a$, $b^* = 2\pi/b$, and $c^* = 2\pi/c$. (See Table I for values of a , b , and c for each sample). The total energy resolution was about 130 meV, and the exact position of the elastic (zero energy loss) line was determined by measuring, for each transferred momentum, a non-resonant spectrum of polycrystalline graphite. All data were recorded at $T = 15 \text{ K}$, each spectrum being the result of 30 to 180 minutes total accumulation (sum of individual spectra of 5 min).

Data Analysis

The data on the parent compound were analyzed using resolution-limited Gaussian line-shapes, as in Ref. 7. Due to the broadening of the lineshape with doping, this analysis does not hold anymore for the other systems. The RIXS intensity is proportional to the dynamical structure factor $S(\vec{Q}, \omega) = [1 + n(\omega, T)]\chi''(\vec{Q}, \omega)$, where $[1 + n(\omega, T)] = (1 - e^{-\frac{\hbar\omega}{k_B T}})^{-1}$ is the Bose factor (step function at $T = 15$ K) and $\chi''(\vec{Q}, \omega)$ is the imaginary part of the spin susceptibility. To take into account the finite lifetime of the excitations in the doped systems, and causality (that imposes $\chi''(\vec{Q}, \omega)$ to be an odd function of energy transfer ω), we modeled $\chi''(\vec{Q}, \omega)$ using an antisymmetrized Lorentzian function, centered on $\omega = \omega_Q$, and of HWHM Γ_Q :

$$\chi''(\vec{Q}, \omega) = \left[\frac{\Gamma_Q}{(\omega - \omega_Q)^2 + (\Gamma_Q^2)} - \frac{\Gamma_Q}{(\omega + \omega_Q)^2 + (\Gamma_Q^2)} \right], \quad (1)$$

convoluted with the Gaussian resolution function (HWHM = 65 meV). Note that in the case of doped systems, we are not able to separate the vibrational contribution to the inelastic response from the magnetic one. This may result in a slight, systematic overestimate of the intrinsic HWHM of the magnetic excitation plotted in Fig. 3c in the main text. As in the undoped case, this contribution does not account for more than 10 % of the total inelastic spectral weight (the inelastic intensities plotted in Fig. 3d all include this vibrational contribution).

In Supplementary Figure 1, the x-ray absorption spectra close to the Cu L_3 absorption edge (normal incidence, π polarization) are shown for each of the investigated compounds. These measurements were taken on beamline ID08 at the European Synchrotron Radiation Facility (ESRF). Since these absorption profiles are essentially identical between the different samples, the self-absorption corrections are not at all critical here. The relative change of the intensities due to self-absorption obtained by doing calculations of the type given in Ref. 8 are smaller than 3 %. The high-energy dd excitation peak (Fig. 1 b,c in the main text) provide an additional calibration standard.

Model calculations

Supplementary Figure 3 shows the cluster shapes used in the numerical computation of the dynamical spin susceptibility of the $t - J$ model. The combination of different cluster shapes displayed in panel a provides access to the momentum points in panel b.

The Eliashberg calculations were performed with the vertex function of the $t - J$ model, $2J\gamma_q + (\epsilon_{k-q} + \epsilon_k)/2$ where $\epsilon_k = -2t(\cos k_x + \cos k_y) - 4t' \cos k_x \cos k_y$ represents the bare electronic dispersion and $\gamma_q = (\cos q_x + \cos q_y)/2$.⁹ The values of the model parameters used in our calculation are $t = 400$ meV, $t' = -t/3$, and $J = 130$ meV. As input we used the simple formula $\chi_q(\omega) = \eta_q/(\omega_q^2 - \omega^2 - i\Gamma_q \omega)$, which provides an excellent description of both the experimental data and the spin susceptibility resulting from the exact-diagonalization calculations. The parameters ω_q and Γ_q denote the paramagnon dispersion and damping (full width at half maximum), respectively. We take $\omega_q = 2J \sqrt{(1 - \gamma_q)(1 + \gamma_q + \omega_Q^2/8J^2)}$ with a spin gap ω_Q at \mathbf{Q}_{AF} . For underdoped YBCO_{6+x}, ω_Q can be directly extracted from INS data. For YBCO₇, where normal-state INS data are not available, the resonant mode below T_c implies $\omega_Q \sim 60$ meV. This value is required to reproduce the experimentally observed resonant mode energy of 40 meV¹⁰ following method described in Ref. 11. Further, $\eta_q = A(1 - \gamma_q)$ with A chosen such that χ'' obeys the corresponding sum rule, as required by the RIXS and INS data.

Supplementary Figure 4 gives an overall picture of T_c as a function of the damping Γ (chosen to be independent of q) and the spin gap at \mathbf{Q}_{AF} . Apparently, non-damped spin waves with a suitably high energy at \mathbf{Q}_{AF} are optimal as the pairing mediators. T_c decreases when the damping increases and/or when the spin gap deviates from its optimum value, $\omega_Q \sim 100$ meV.

-
1. Hinkov, V. *et al.* Two-dimensional geometry of spin excitations in the high-transition-temperature superconductor YBa₂Cu₃O_{6+x} *Nature* **430**, 650-653 (2004).
 2. Song, Y. T. *et al.* Ambient-condition growth of superconducting YBa₂Cu₄O₈ single crystals using KOH flux. *J. Cryst. Growth* **300**, 263-266 (2007).
 3. Sun, G. L., Song, Y. T. & Lin, C. T. Investigation of YBa₂Cu₄O₈ single crystal growth by KOH flux. *Supercond. Sci. Technol.* **21**, 125001 (2008).
 4. Salluzzo, M. *et al.* Thickness effect on the structure and superconductivity of Nd_{1.2}Ba_{1.8}Cu₃O_z epitaxial films. *Phys. Rev. B* **72**, 134521 (2005).
 5. Strocov, V. N. *et al.* High-resolution soft X-ray beamline ADDRESS at the Swiss Light Source for resonant inelastic X-ray scattering and angle-resolved photoelectron spectroscopies. *J. Synchrot. Radiat.* **17**, 631-643 (2010).
 6. Ghiringhelli, G. *et al.* SAXES, a high resolution spectrometer for resonant x-ray emission in the

- 400-1600 eV energy range. *Rev. Sci. Instrum.* **77**, 113108 (2006).
7. Braicovich, L. *et al.* Magnetic Excitations and Phase Separation in the Underdoped $\text{La}_{2-x}\text{Sr}_x\text{CuO}_4$ Superconductor Measured by Resonant Inelastic X-Ray Scattering. *Phys. Rev. Lett.* **104**, 077002 (2010).
 8. Eisebitt, S. *et al.* Determination of absorption coefficients for concentrated samples by fluorescence detection. *Phys. Rev. B* **47**, 14103-14109 (1993).
 9. Prelovšek P. and Ramšak, A. Spectral functions and the pseudogap in the t-J model *Phys. Rev. B* **63**, 180506(R) (2001).
 10. Fong, H. F. *et al.* Polarized and unpolarized neutron-scattering study of the dynamical spin susceptibility of $\text{YBa}_2\text{Cu}_3\text{O}_7$. *Phys. Rev. B* **54**, 6708-6720 (1996).
 11. Prelovšek, P. & Sega, I. Magnetic collective mode in underdoped cuprates: A phenomenological analysis. *Phys. Rev. B* **74**, 214501 (2006).

Sample	a	b	c	Transition Temperature
$\text{Nd}_{1.2}\text{Ba}_{1.8}\text{Cu}_3\text{O}_6$	3.905 Å	3.905 Å	11.85 Å	$T_N > 300$ K
$\text{Nd}_{1.2}\text{Ba}_{1.8}\text{Cu}_3\text{O}_7$	3.885 Å	3.92 Å	11.7 Å	$T_c = 65$ K
$\text{YBa}_2\text{Cu}_3\text{O}_{6.6}$	3.82 Å	3.87 Å	11.7 Å	$T_c = 61$ K
$\text{YBa}_2\text{Cu}_4\text{O}_8$	3.84 Å	3.87 Å	27.25 Å	$T_c = 80$ K
$\text{YBa}_2\text{Cu}_3\text{O}_7$	3.817 Å	3.884 Å	11.681 Å	$T_c = 90$ K

Table I: **Supplementary Material** Lattice parameters and transition temperatures of the samples investigated here.

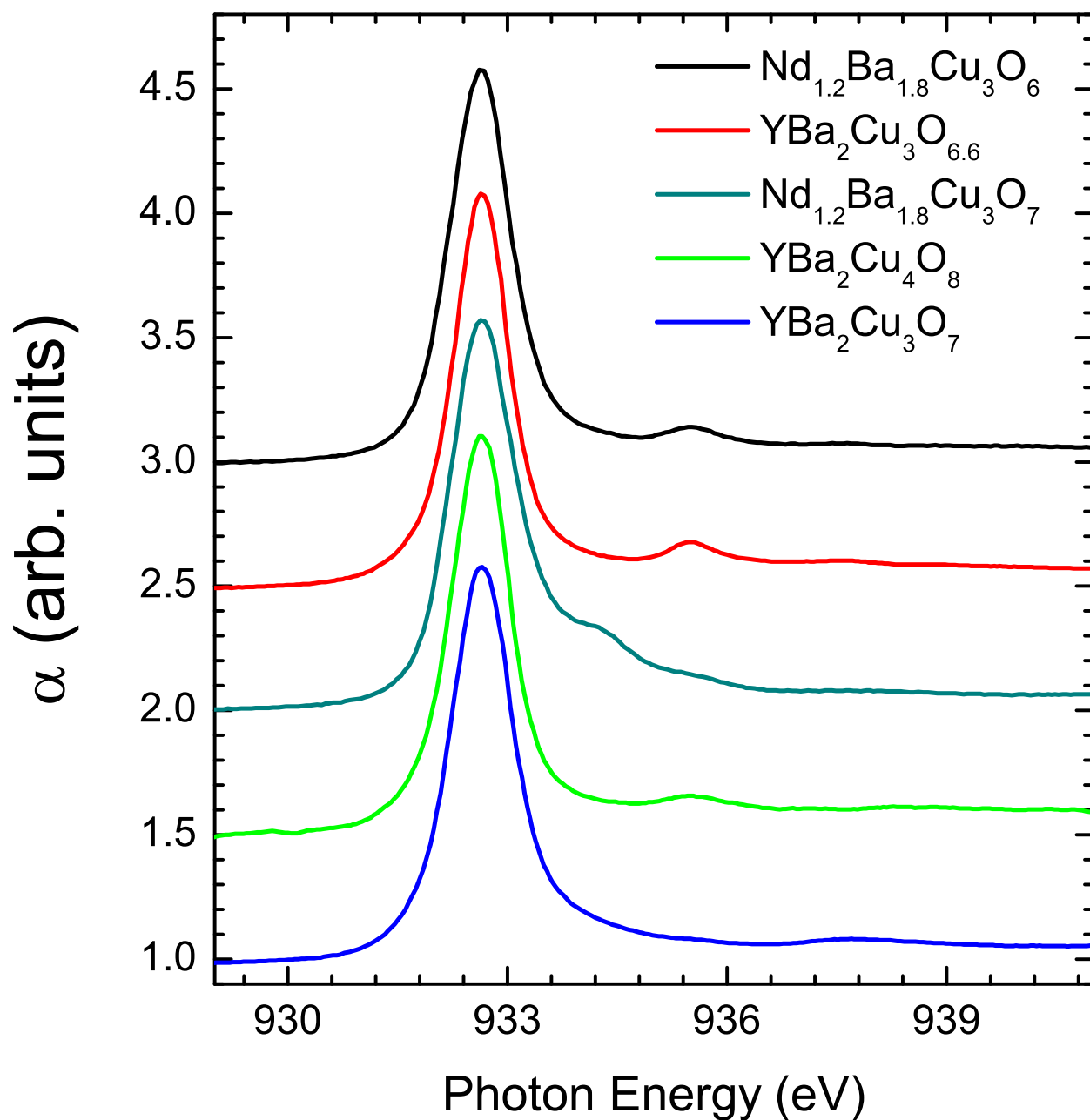


Fig. 5: **Supplementary Material** Cu L_3 edge X-ray absorption spectra of all the investigated compounds measured with total electron yield (normal incidence, π polarization). Spectra have been vertically shifted by 0.5 for clarity.

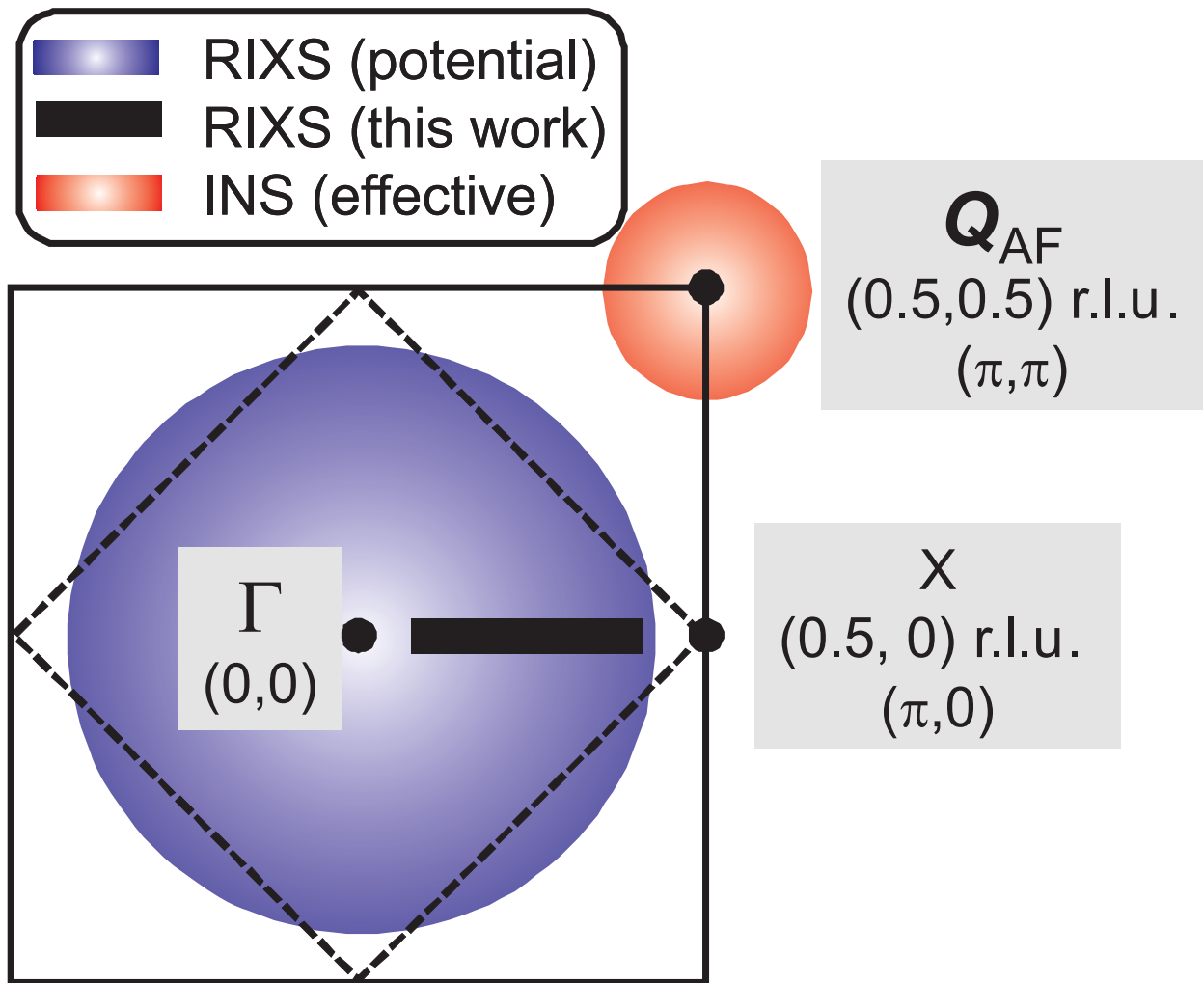


Fig. 6: **Supplementary Material** Sketch of the accessible reciprocal space with RIXS experiments at the Cu L_3 edge. The black line represents the region explored in this work. In red we have represented the typical region of the reciprocal space studied INS in doped YBCO.

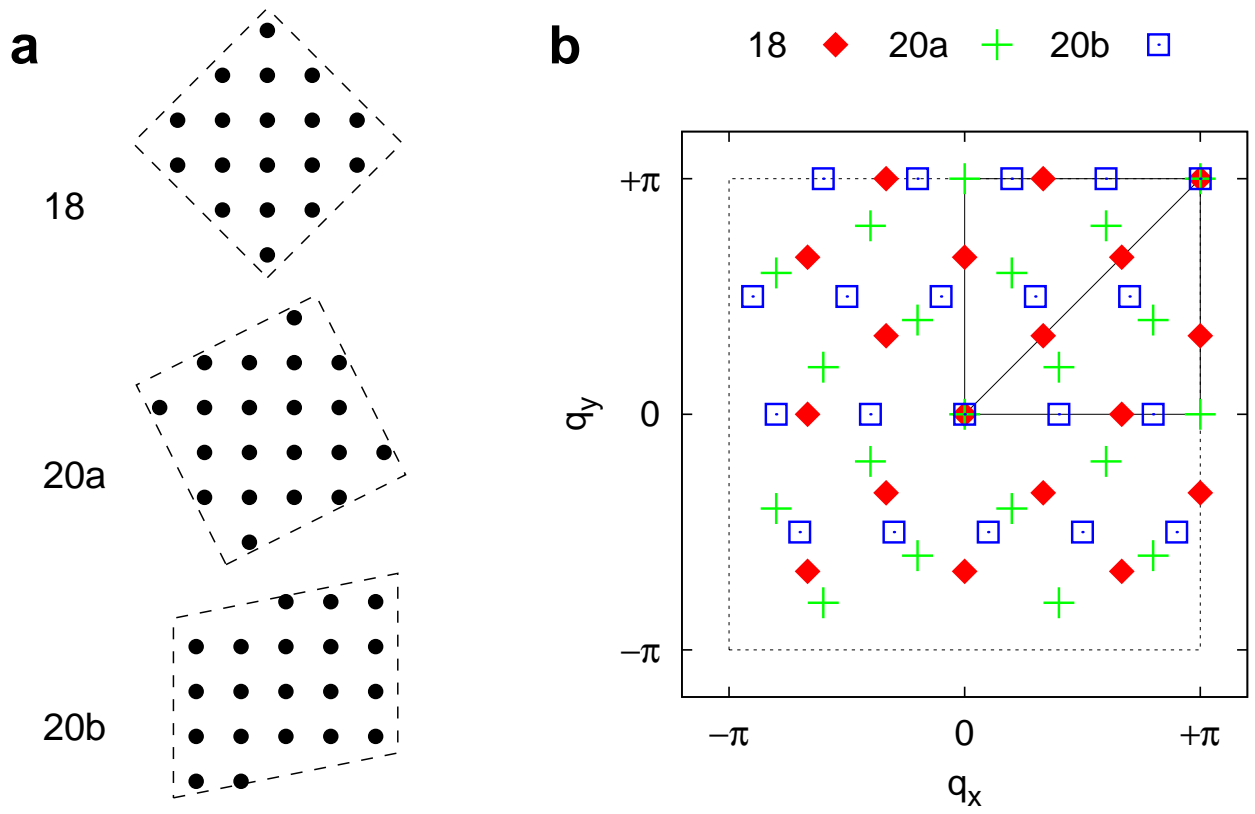


Fig. 7: **Supplementary Material** a) Cluster shapes used to compute the spin fluctuation spectra of Fig. 4 in the main text. b) Non-equivalent \mathbf{q} -vectors accessible to calculations on the different clusters.

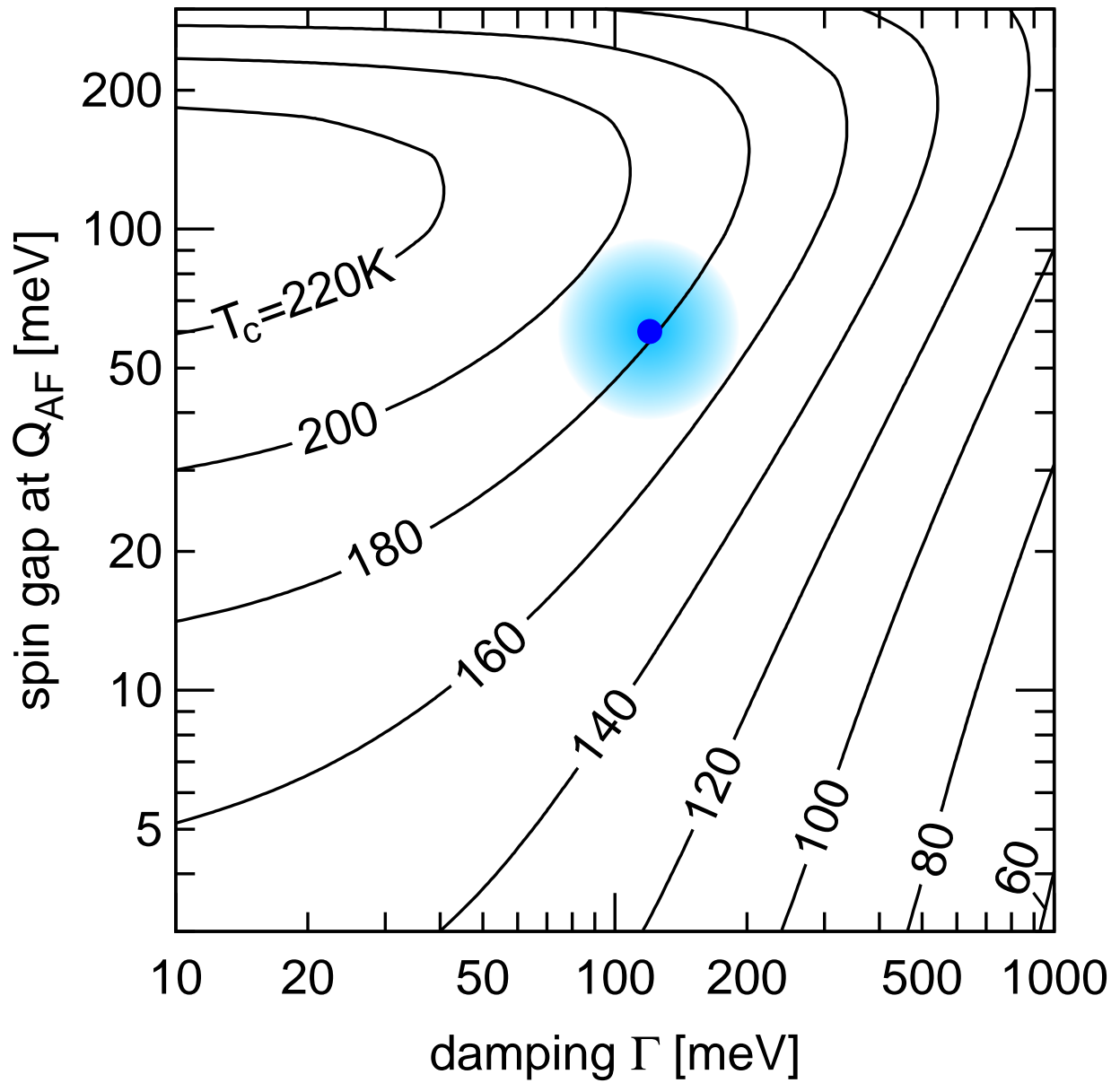


Fig. 8: **Supplementary Material** Contour plot of the superconducting transition temperature resulting from the Eliashberg calculation as a function of the spin gap at wave vector Q_{AF} and the damping parameter Γ . The values appropriate for $YBCO_7$ are marked in blue.